




Article

Chlorosubstituted Copper Phthalocyanines: Spectral Study and Structure of Thin Films

Alexandr Sukhikh ¹, Dmitry Bonegardt ¹, Darya Klyamer ¹, Pavel Krasnov ² and Tamara Basova ^{1,*}

¹ Nikolaev Institute of Inorganic Chemistry SB RAS, 3 Lavrentiev Pr., 630090 Novosibirsk, Russia; a_sukhikh@niic.nsc.ru (A.S.); bonegardt@niic.nsc.ru (D.B.); klyamer@niic.nsc.ru (D.K.)

² Laboratory of Non-Linear Optics and Spectroscopy, Siberian Federal University, 79 Svobodny Prospect, 660041 Krasnoyarsk, Russia; kpo1980@gmail.com

* Correspondence: basova@niic.nsc.ru; Tel.: +7-383-330-89-57

Academic Editor: Simona Collina

Received: 17 March 2020; Accepted: 31 March 2020; Published: 1 April 2020



Abstract: In this work, the tetra-, octa- and hexadecachloro-substituted copper phthalocyanines CuPcCl_x (where x can equal 4, 8 or 16) were investigated by the methods of vibrational (IR and Raman) spectroscopy and X-ray diffraction. The assignment of the most intense bands, both in IR and Raman spectra, was carried out on the basis of DFT calculations. The structure of a CuPcCl₄ single crystal grown by sublimation in vacuum was refined for the first time. The effect of chloro-substitution on the structure of CuPcCl_x thin films deposited in a vacuum onto a glass substrate at 50 and 200 °C was studied. It was shown that CuPcCl₄ formed polycrystalline films with the preferential orientation of the (100) crystallographic plane of crystallites parallel to the substrate surface when deposited on a substrate at 50 °C. Introduction of more Cl-substituents into the phthalocyanine macrocycle leads to the formation of amorphous films on the substrates at 50 °C. At the elevated substrate temperature, the growth of polycrystalline disordered films was observed for all three copper phthalocyanines.

Keywords: phthalocyanines; single crystal structure; thin films; X-ray diffraction; vibrational spectra; DFT calculations

1. Introduction

Metal phthalocyanines (MPcs) attract the wide attention of researcher in various areas of materials science, chemistry and electronics. For their application in different electronic devices, they should be prepared as thin layers with an easily reproducible structure and ordering. Although halogen-substituted phthalocyanines were synthesized a long time ago [1], the interest in their thin films has increased again in recent years. This is primarily due to their comparatively high charge carriers' mobility and *n*-type semiconducting behavior [2]. The literature analysis shows that a number of works are devoted to the investigation of fluoro-substituted metal phthalocyanines, as active layers of organic field-effect transistors (OFETs) [3–5]. Note that the structural feature and the orientation of molecules relative to the substrate surface in their films have a noticeable effect on the mobility of charge carriers and other OFET characteristics [6,7]. For instance, the mobility of charge carriers in OFETs on the basis of CuPcF₁₆ can vary from 10^{−3} [8] to 0.27 cm²/V·s [6] in dependence on the structure of films and the dielectric layers. The structure of single crystals and thin films of fluorinated metal phthalocyanines MPcF_x (M = Co, Zn, Pd, VO; x = 4, 16) were studied in a series of our previous publications [9–11].

The literature analysis shows that the most works on chlorinated metal phthalocyanines are devoted to their synthesis [12–14], behavior in solutions [15] and applications as pigments [16,17]. At the same time, the films of chloro-substituted phthalocyanines are also considered as active layers of

molecular electronic devices, however such works on the investigation of the structure and properties of their films are sporadic. For example, Pakhomov et al. mentioned that CuPcCl_4 films can be deposited by vacuum sublimation, but did not characterize them [18]. Several works were devoted to the epitaxial growths of monolayers or ultrathin films on graphite, graphene and KBr (001), and their investigation by the methods of high-resolution electron microscopy [19–22] and photoelectron spectroscopy [23]. Haruta et al. [24] studied grain boundaries in the thin films of CuPcCl_{16} using an aberration-corrected scanning transmission electron microscope combined with electron energy-loss spectroscopy. Fryer [25] determined the parameters of crystal cell of CuPcCl_x ($x = 4, 8, 16$) using the method of electron diffraction.

Similarly to unsubstituted and fluoro-substituted derivatives, chloro-substituted metal phthalocyanines exhibit semiconductor properties. According to DFT calculations, the HOMO and LUMO energy levels of CuPcCl_x decrease in comparison with unsubstituted CuPc derivatives [26,27]. Koshy et al. [28] investigated the effect of annealing temperature on the optical band gap of FePcCl_{16} films, and considered their possible applications as active layers of molecular electronic devices. Anchar et al. [29] have shown that the conductivity of CuPcCl_4 pellets is about four orders of magnitude higher than that of unsubstituted CuPc. Ling, Bao and Erk determined that the carrier mobility of a CuPcCl_{16} film deposited at an elevated substrate temperature in air-stable *n*-channel transistors was $\sim 10^{-2} \text{ cm}^2 \text{ V}^{-1} \text{ s}^{-1}$ [30]. It is known that the electrical properties of phthalocyanines and other molecular crystals are dependent upon the phase composition, morphology and orientation of molecules in thin films [6,7,28]. It is worth mentioning that in most of the abovementioned articles, the structure of thin films MPcCl_x was not studied. For this reason, the study of the structural features of MPcCl_x films deposited under different conditions is an important task. In addition to X-ray diffraction techniques, spectral methods, including IR and Raman spectroscopies, are also very informative methods for the investigation of the structural features of phthalocyanine films. For this reason, the detailed assignment of vibrations in IR and Raman spectra is a vital issue.

In this work, the tetra-, octa- and hexadecachloro-substituted copper phthalocyanines CuPcCl_x ($x = 4, 8, 16$) were investigated by the methods of vibrational (IR and Raman) spectroscopy and X-ray diffraction. The assignment of the most intense bands, both in IR and Raman spectra, was carried out on the basis of DFT calculations. The structure of a CuPcCl_4 single crystal was refined for the first time. The effect of chloro-substitution on the structure of CuPcCl_x thin films deposited in vacuum onto the substrate at different temperatures was studied.

2. Results and Discussion

2.1. Single Crystal Structure of CuPcCl_4

A single crystal of CuPcCl_4 in the form of a small needle ($0.15 \text{ mm} \times 0.03 \text{ mm} \times 0.03 \text{ mm}$) of dark purple color was selected from a polycrystalline crust formed on the side of a glass ampule during the gradient vacuum sublimation of the product obtained after the synthesis. The unit cell parameters at 150 and 298 K, and the crystal structure refinement statistics are given in Table 1. CuPcCl_4 crystallizes in a monoclinic crystal system, with a $P2_1/c$ space group, and $Z = 2$. It is worth mentioning that different unit cell parameters for CuPcCl_4 were reported by Honigmann et al. [31] ($a = 26.3 \text{ \AA}$, $b = 27.8 \text{ \AA}$, $c = 27.8 \text{ \AA}$, $\beta = 94^\circ$, $P2_1/a$ space group) and Fryer [25] ($a = 27.4 \text{ \AA}$, $b = 27.4 \text{ \AA}$, $c = 3.65 \text{ \AA}$, $P4$ space group or $C2/c$ space group with $\beta = 90^\circ$). Although these unit cell parameters differ significantly from those obtained from a single crystal in this work, this does not necessarily mean that CuPcCl_4 has several different polymorphs. In the first case, the lattice parameter c appears to be doubled (27.8 \AA instead of 13.9 \AA), and the parameter b is multiplied by 8 (27.8 \AA instead of 3.48 \AA), while the lattice parameter a and the monoclinic angle β agree fairly well with the single-crystal data.

In the second case, the unit cell parameters of CuPcCl_4 were derived from electron diffraction patterns, which have the lower accuracy compared to X-ray diffraction. Thus, the difference between

the single-crystal data and the reported unit cell parameters may be caused by instrumental limitations and an incorrect assignment of Miller indices.

Packing diagrams of CuPcCl₄ molecules are shown in Figure 1. CuPcCl₄ molecules are almost flat (the maximum deviation from the mean squared plane is 0.12 Å for one of the chlorine atoms), being packed in columns along the *b* axis (Figure 1b), and arranged in the herringbone configuration (Figure 1a).

Table 1. Unit cell parameters and refinement statistics for CuPcCl₄.

Empirical Formula	C ₃₂ H ₁₂ Cl ₄ CuN ₈	
Formula weight	713.84	
Temperature/K	150	298
Crystal system	monoclinic	monoclinic
Space group	P2 ₁ /c	P2 ₁ /c
<i>a</i> /Å	14.0052(9)	14.080(4)
<i>b</i> /Å	3.6376(3)	3.6823(8)
<i>c</i> /Å	26.5123(18)	26.693(5)
α/°	90	90
β/°	94.893(3)	94.636(20)
γ/°	90	90
Volume/Å ³	1345.76(17)	1379.4(5)
<i>Z</i>	2	2
ρ _{calc} /g/cm ³	1.762	1.806
Reflections collected	12242	N/A
Independent reflections	2580 (R _{int} = 9.05%)	N/A
Data/restraints/parameters	2508/0/225	N/A
Goodness-of-fit on F ²	1.010	N/A
R indices [<i>I</i> > 2σ (<i>I</i>)]	R ₁ = 4.90%, wR ₂ = 9.02%	N/A
R indices [all data]	R ₁ = 12.03%, wR ₂ = 11.05%	N/A
CCDC No.	1972791	N/A

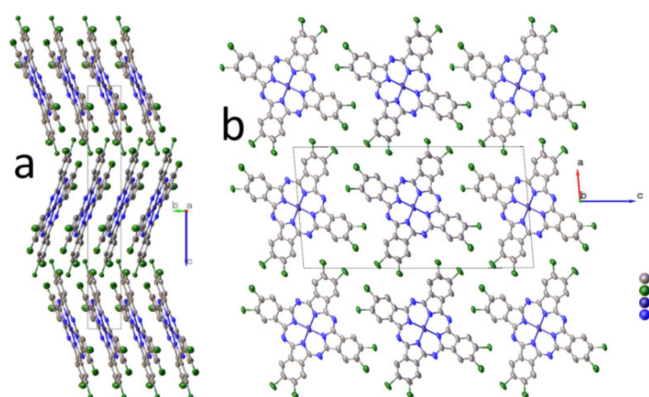


Figure 1. Packing diagrams of CuPcCl₄ molecules along the *a* axis (a) and *b* axis (b). Chlorine atoms partially occupy eight positions (0.514/0.486 and 0.516/0.484 for Cl1/Cl2 and Cl3/Cl4, respectively).

Chlorine atoms partially occupy eight positions (0.514/0.486 and 0.516/0.484 for Cl1/Cl2 and Cl3/Cl4, respectively) because the synthesized CuPcCl₄ consists of four regioisomers co-crystallizing in one crystal phase. The distance between two molecules (the mean-square plane through all atoms in the molecule, except hydrogen) in a stack is 3.376 Å, while the stacking angle (the angle between the normal to the plane of the molecule and *b*-axis) is 21.88° (27° as reported in Fryers work [25]). The angle between two molecules in adjacent stacks is 43.76°. These values differ significantly from those reported for a stable β-polymorph of unsubstituted copper phthalocyanine (3.342 Å and 45.76°) [32], in which

molecules in adjacent stacks are oriented almost perpendicularly to each other, and for CuPcF₄ [11] (3.381 Å and 24.29°), in which molecules in adjacent stacks are parallel to each other. A similar stacking pattern, however, is observed in γ -CuPc (3.386 Å and 27.37°) [33]. Although γ -CuPc crystallizes in the other space group (C2/c), its unit cell parameters ($a = 26.3330$ Å, $b = 3.8133$ Å, $c = 23.7118$ Å, $\beta = 94.2845^\circ$) are similar to CuPcCl₄.

Figure 2 shows the Hirshfeld surface for an individual CuPcCl₄ molecule, mapped with different properties (shape index, curvedness and normalized contact distance), as well as the fingerprint plot for all intermolecular contacts with chlorine atoms that occupy 32.4% of the entire Hirshfeld surface. The Hirshfeld surface mapped with the shape index (Figure 2a) is shown with the adjacent molecule in the stack, superimposed over it.

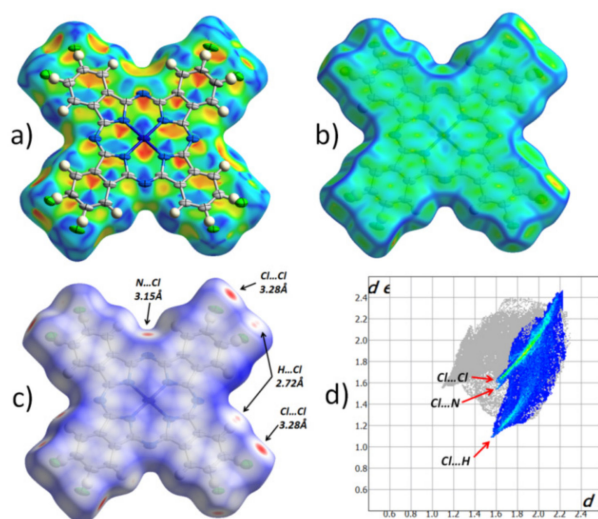


Figure 2. Hirshfeld surface for CuPcCl₄ molecule, mapped with the shape index (a), curvedness (b), normalized contact distance (d_{norm} , $-0.15 \dots +1$ range) (c) and the fingerprint plot for all intermolecular contacts with chlorine atoms (d).

Pairs of red and blue triangles (Figure 2a), located in the shape of an hourglass, are visible inside each of the benzene and pyrrole rings, as well as in all four quadrants of the central phthalocyanine macrocycle. These features together with the uniform flat surface (Figure 2b) clearly show π - π interaction between CuPcCl₄ molecules in one stack. Moreover, each individual aromatic segment of one molecule interacts with the same segment of a neighboring molecule. The same type of π - π interaction was previously observed in CuPcF₄, but not in β -CuPc [11]. The Hirshfeld surface mapped with the normalized contact distance (Figure 2c; d_{norm} , $-0.15 \dots +1$ range) shows that there are no other close contacts between the molecules in one stack. However, unlike CuPcF₄ and β -CuPc, which have almost no close contacts, there are several close contacts between CuPcCl₄ molecules in adjacent stacks, and they all involve peripheral chlorine atoms. The fingerprint plot (Figure 2d) shows three distinct groups of close contacts, viz. 3.28 Å Cl..Cl, 3.15 Å Cl..N $_{\beta}$, 2.72 Å Cl..H.

The most prominent close contacts are Cl..Cl ones, which are ~ 0.2 Å shorter than the sum of van der Waals radii of two chlorine atoms. However, these contacts are not necessarily present in each individual CuPcCl₄ molecule, because all atomic positions of chlorine are only partially occupied. This may also explain the strange appearance of thermal ellipsoids (Figure 2a), such that they are all elongated in the same direction. It is possible that, depending on the presence of chlorine atoms in certain positions associated with Cl..Cl close contacts, CuPcCl₄ molecules can shift slightly inside the stack to minimize the stress caused by close contacts.

2.2. Vibrational Spectra

The IR and Raman spectra of CuPcCl_x ($x = 4, 8, 16$) are given in Figures 3 and 4, respectively. The spectra of unsubstituted CuPc are also given for comparison. The assignment of vibrational spectra was based on the results of quantum chemical calculations. The calculated spectra are in good agreement with the experimental ones. A comparison of the calculated and experimental IR spectrum of CuPcCl_4 is presented in Figure 5 as an example. Tables S1–S4 (Supplementary Materials) summarize the experimental and calculated wavenumbers, as well as the assignment of the most intense bands in IR and Raman spectra of CuPcCl_x derivatives.

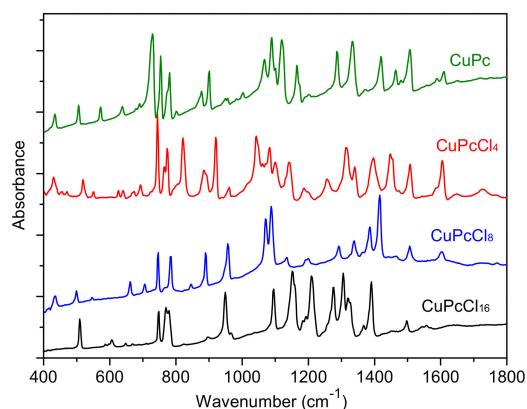


Figure 3. Infrared (IR) spectra of CuPcCl_x ($x = 0, 4, 8, 16$).

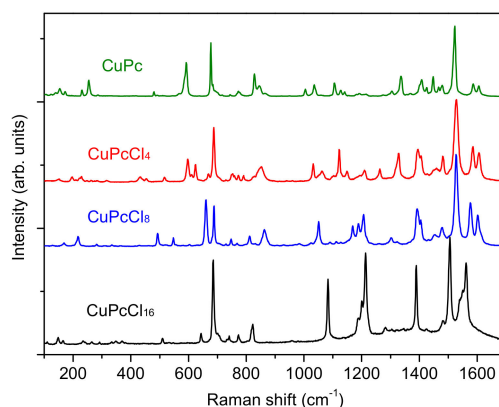


Figure 4. Raman spectra of CuPcCl_x ($x = 0, 4, 8, 16$).

CuPcCl_4 and CuPcCl_8 are planar molecules of D_{4h} and C_{4h} point group symmetry, while the introduction of 16 chlorine substituents into the phthalocyanine macrocycles leads to a non-planar distortion of the CuPcCl_{16} macrocycle, and as a result, a decrease of the molecule symmetry to D_{2d} .

A comparison of experimental and DFT-optimized bond lengths in CuPcCl_x molecules is given in Table 2.

The introduction of bulky Cl-substituents to the phthalocyanine macrocycle leads to the shift of some modes in the range from 1350 to 1620 cm^{-1} to the lower wavenumbers compared to CuPc [34]. These modes are attributed to C=C and C=N stretching vibrations and isoindole deformations. For example, the mode at 1608 cm^{-1} in the IR spectrum of CuPc attributed to C=C stretchings shifts to 1605 , 1602 and 1558 cm^{-1} for CuPcCl_4 , CuPcCl_8 and CuPcCl_{16} , respectively, due to the induction (-I) effects of electron-withdrawing Cl-atoms. The introduction of Cl-substituents causes the change of both the intensity and wavenumbers of the most bands in the range from 700 to 1300 cm^{-1} because of the change of the forms of the corresponding vibrations and the strong contributions of C–Cl vibrations. This is especially noticeable in the case of CuPcCl_8 and CuPcCl_{16} derivatives. Even the group of bands

at 500–900 cm^{-1} , where the most vibrations are attributed to macro-ring deformations along with Cu-N $_{\alpha}$ stretchings, is not left unchanged.

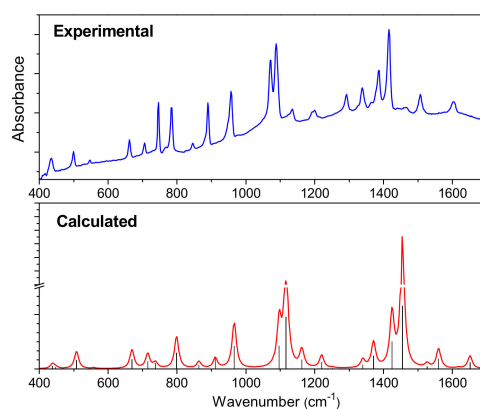


Figure 5. Experimental and calculated IR spectra of CuPcCl₄.

Table 2. Bond lengths (Å) in CuPcCl_x (x = 4, 8, 16) molecules.

Bond	CuPcCl ₄		CuPcCl ₈	CuPcCl ₁₆
	Experimental	Calculated		
Cu-N $_{\alpha}$	1.942	1.951	1.951	1.950
C $_{\alpha}$ -N $_{\alpha}$	1.372	1.377	1.376	1.372
C $_{\alpha}$ -N $_{\beta}$	1.332	1.324	1.324	1.322
C $_{\alpha}$ -C $_{\beta}$	1.454	1.456	1.457	1.465
C $_{\beta}$ -C $_{\beta}$	1.392	1.405	1.404	1.412
C $_{\beta}$ -C $_{\gamma}$	1.391	1.396	1.392	1.400
C $_{\gamma}$ -C $_{\delta}$	1.376	1.392	1.394	1.404
C $_{\delta}$ -C $_{\delta}$	1.393	1.408	1.418	1.415
C $_{\gamma}$ -H	n/a	1.084	1.084	-
C $_{\delta}$ -H	n/a	1.084	-	-
C $_{\gamma}$ -Cl	-	-	-	1.736
C $_{\delta}$ -Cl	1.682	1.758	1.746	1.732

Similar changes are also observed in the Raman spectra. The spectra of CuPc and CuPcCl₄ are similar, whereas the introduction of 8 and 16 chlorine substituents causes noticeable shifts and the change of intensities of most vibrations. The bands belonging to C=C stretching vibrations at 1607 and 1589 cm^{-1} observed in the case of CuPc shift to the lower wavenumbers in the Raman spectra of CuPcCl₄, CuPcCl₈ and CuPcCl₁₆. The strong bands at 1528 cm^{-1} in the spectra of CuPcCl₄ and CuPcCl₈, corresponding to C $_{\alpha}$ -N $_{\beta}$ and C $_{\beta}$ -C $_{\beta}$ stretchings, are not shifted relative to the corresponding band in the spectrum of CuPc, while in the spectrum of CuPcCl₁₆, this band is observed at 1506 cm^{-1} . When compared with the spectra of CuPc and CuPcCl₄, the intensities of bands at 492, 660 and 1050 cm^{-1} in the CuPcCl₈ spectrum, and at 643 and 1078 cm^{-1} in the CuPcCl₁₆ spectrum, increase due to the contribution of C-Cl stretchings to these vibrations. It is interesting to mention that the totally symmetric bands with dominating contribution of C $_{\alpha}$ -N $_{\beta}$ -C $_{\alpha}$ deformation do not practically change and locate at 689, 688 and 685 cm^{-1} in the spectra of CuPcCl₄, CuPcCl₈ and CuPcCl₁₆. At the same time the wavenumbers of totally symmetric bands located at 820–850 cm^{-1} vary because of different forms of these vibrations: in the Raman spectra of CuPcCl₄ and CuPcCl₈, these vibrations at 828 and 832 cm^{-1} are associated with macro-ring breathing with the contribution of C $_{\beta}$ -C $_{\gamma}$ -H, while

in the case of CuPcCl_{16} , this mode lies at 821 cm^{-1} , and involves not only macro-ring and $\text{C}_\beta\text{-C}_\gamma\text{-H}$ deformations, but also $\text{C}_\gamma\text{-Cl}$ and $\text{C}_\delta\text{-Cl}$.

2.3. XRD Study of CuPcCl_4 , CuPcCl_8 and CuPcCl_{16} Thin Films

Thin films of CuPcCl_4 , CuPcCl_8 and CuPcCl_{16} were deposited onto glass substrates at two different temperatures 50 and 200 °C. The diffraction patterns for CuPcCl_4 , CuPcCl_8 and CuPcCl_{16} polycrystalline powders and thin films are shown in Figure 6.

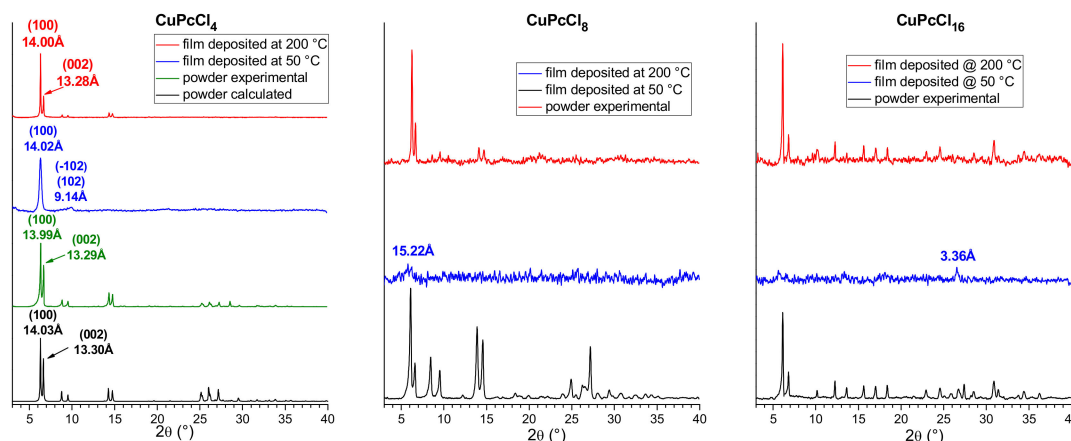


Figure 6. Diffraction patterns of CuPcCl_4 , CuPcCl_8 and CuPcCl_{16} polycrystalline powders and thin films deposited at 50 °C and 200 °C.

CuPcCl_4 powder was compared with the diffraction pattern calculated using single-crystal data obtained at 150 K and unit cell parameters measured from the same single crystal at room temperature (298 K). The experimental peak positions and intensities match well with the calculated ones, and no additional diffraction peaks are observed, indicating that the CuPcCl_4 powder is single phase. A single strong diffraction peak is observed on the diffraction pattern of CuPcCl_4 thin film deposited onto a substrate at 50 °C. Since the 2θ position of this peak almost perfectly coincides with the (100) peak in the calculated diffraction pattern of the powder, it is possible to conclude that this thin film consists of the same crystalline phase as the bulk polycrystalline powder, but has a strong preferred orientation with the (100) crystallographic plane of the majority of crystallites oriented parallel to the substrate surface. The inclination angle of CuPcCl_4 molecules relative to the substrate surface (Figure 7) was estimated to be 79.2° (cf. 76.6° for CuPc and 82.7° for CuPcF_4). In addition to the strong (100) peak, the diffraction pattern shows a weak and blurred diffraction peak with the interplane distance of 9.14 \AA , which can be attributed to the planes (-102) and (102) , which means that the preferred orientation of CuPcCl_4 is not ideal.

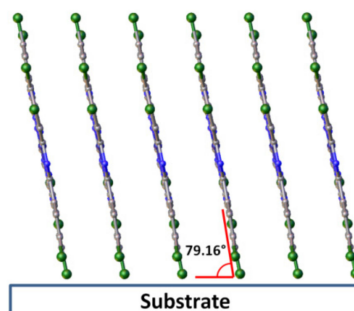


Figure 7. Orientation of CuPcCl_4 molecules relative to the substrate surface in thin films.

Multiple diffraction peaks are observed on the diffraction pattern of a CuPcCl_4 film deposited on the substrate at 200 °C, indicating that it has no preferred orientation (Figure 6). 2θ positions of all observed peaks also coincide well with the calculated pattern of the powder. This means that CuPcCl_4 films consist of the same crystal phase, and there is no evidence of other polymorphic modifications. CuPcCl_8 and CuPcCl_{16} thin films deposited on the substrates at 50 °C are amorphous (Figure 6). Their diffraction pattern contains almost no diffraction peaks, except for very weak peaks at 15.22 Å for CuPcCl_8 , and at 3.36 Å for CuPcCl_{16} . On the other hand, the films deposited on the substrates at 200 °C are crystalline, and multiple diffraction peaks are observed on their diffraction patterns. 2θ positions of the diffraction peaks of these films coincide with the corresponding powder diffraction patterns, which means that the CuPcCl_8 and CuPcCl_{16} films deposited at 200 °C have the same phase composition as their polycrystalline powders.

The unit cell parameters measured using electron microdiffraction [35] are available in the literature for CuPcCl_{16} : $a = 19.62$ Å, $b = 26.04$ Å, $c = 3.76$ Å, $\beta = 116.5^\circ$, C2/c or C2/m space group. Based on these data, the CuPcCl_{16} diffraction pattern was indexed, and the unit cell parameters were refined using the 2θ positions of the diffraction peaks measured from the powder diffraction pattern (see Table S6). The refined unit cell parameters for CuPcCl_{16} are: $a = 19.16(2)$ Å, $b = 26.03(3)$ Å, $c = 3.695(3)$ Å, $\beta = 114.55(1)^\circ$, $V = 1675(3)$ Å³. All diffraction peaks on the CuPcCl_{16} XRD pattern are indexed within the specified unit cell parameters, which means that both the film deposited on the substrate at 200 °C and the bulk powder consist of one crystal phase. The only available XRD data for CuPcCl_8 are the 2θ positions of several strongest diffraction peaks measured from the powder diffraction pattern (6.1° , 6.6° , 8.5° , 9.5° , 14.0° , 14.5° , 24.9° and 27.1° , $\text{CuK}\alpha$ radiation) [36], which match well with the strongest peaks observed in our XRD data. Therefore, the appropriate unit cell parameters for CuPcCl_8 were found using the DICVOL14 indexing program [37]. Since V/Z ratios (volume of one molecule) of CuPcCl_4 and CuPcCl_{16} are known (689.7 and 859.6 Å³, respectively), they were used as the lower and upper limits for the volume of the CuPcCl_8 molecule in the search process. The obtained unit cell parameters for CuPcCl_8 are: $a = 8.01(1)$ Å, $b = 13.64(2)$ Å, $c = 14.75(2)$ Å, $\alpha = 82.03(7)^\circ$, $\beta = 82.03(9)^\circ$, $\gamma = 80.59(8)^\circ$, $V = 1564(3)$ Å³, P-1 space group. All diffraction peaks on the CuPcCl_8 XRD pattern with their 2θ positions, intensities and assigned hkl indices are listed in Table S7. It is worth mentioning that another octa-halogenated phthalocyanine, ZnPcF_8 , has similar unit cell parameters ($a = 8.196$ Å, $b = 11.493$ Å, $c = 13.995$ Å, $\alpha = 78.460^\circ$, $\beta = 73.501^\circ$, $\gamma = 89.078^\circ$) [38], determined from single crystal data. This may serve as indirect confirmation that the indexing was correct, and that CuPcCl_8 may have a molecular packaging style similar to ZnPcF_8 .

3. Materials and Methods

CuPcCl_x derivatives were synthesized by the method of template synthesis from the corresponding chloro-substituted phthalonitriles (Sigma Aldrich, Saint Louis, USA) and CuCl [39]. For purification the obtained powders were sublimed in vacuum (10^{-5} Torr) twice. The sublimation temperatures were 430, 460 and 490 °C for CuPcCl_4 , CuPcCl_8 and CuPcCl_{16} , respectively. Thin films of CuPcCl_x ($x = 4, 8, 16$) were deposited by physical vapor deposition onto glass substrates at two different substrate temperatures of 50 and 200 °C. The nominal thickness of the deposited films varied in the range of 100–150 nm.

IR spectra of CuPcCl_x in KBr pellets were recorded with a Vertex 80 FTIR spectrometer (Ettlingen, Germany) while those Raman spectra of the CuPcCl_x powders were measured with a LabRAM Horiba single spectrometer (HORIBA, Montpellier, France) (488 nm line of an Ar+ laser).

The crystal structure of CuPcCl_4 was determined using a Bruker X8 single-crystal diffractometer (Billerica, MA, US) (a $\text{MoK}\alpha$ sealed tube with a graphite monochromator and Apex II CCD detector). The temperature of crystal was kept at 150 K by an Oxford Cryosystems Cryostream 800 (Oxford, United Kingdom) plus open-flow nitrogen gas cooler. Data collection strategy consisted of conventional φ - and ω -scans with 0.5° wide frames. The Apex3 v.2018-7.2 (Madison, Wisconsin, USA) software package [40] was used for data reduction and absorption correction. The crystal structure was processed

in Olex2 v.1.2.10 (Durham, United Kingdom) [41] with SHELXT–2018/2 (Göttingen, Germany) [42] and SHELXL–2018/3 (Göttingen, Germany) [43] used for the initial structure solution and subsequent refinement, respectively. Additionally, the unit cell parameters of the same crystal were measured at 298 K using 119 individual reflections. Hirshfeld surfaces mapped with different properties (curvedness, shape index, normalized contact distance) were generated in CrystalExplorer 17.5 (Perth, Western Australia, Australia) [44] using a Tonto v.17.04 computational chemistry package (Perth, Western Australia, Australia) [45]. Diffraction patterns of bulk polycrystalline powders and thin films were recorded on a Shimadzu XRD–7000 powder diffractometer (Kyoto, Japan) (a CuK α sealed tube with Ni β -filter, Bragg-Brentano geometry with a vertical θ - θ goniometer and OneSight SSD detector).

Quantum-chemical calculations of geometries and IR and Raman spectra of CuPcCl $_x$ ($x = 4, 8, 16$) molecules were carried out by the DFT B3LYP/6–31G(d,p) method [46–49] in the frame of spin-unrestricted Kohn–Sham theory (UKS) with use of GAMESS software (version 20.04.2017 (R1), Ames, IA, USA) [50]. Doublet spin states only were considered in all three cases. Geometry relaxation of the CuPcCl $_4$, CuPcCl $_8$ and CuPcCl $_{16}$ molecules was constrained by their corresponding symmetries, such as C $_{4h}$, D $_{4h}$ and D $_{2d}$.

4. Conclusions

In this work, tetra-, octa- and hexadecachloro-substituted copper phthalocyanines CuPcCl $_x$ ($x = 4, 8, 16$) were investigated by the methods of vibrational (IR and Raman) spectroscopy and X-ray diffraction. The assignment of the most intense bands both in IR and Raman spectra was carried out on the basis of DFT calculations. It was shown that CuPcCl $_4$ and CuPcCl $_8$ were planar molecules of D $_{4h}$ and C $_{4h}$ point group symmetry, while the introduction of 16 chlorine substituents into the phthalocyanine macrocycles led to a non-planar distortion of the CuPcCl $_{16}$ macrocycle, and as a result, a decrease of the molecule symmetry to D $_{2d}$. The introduction of Cl-substituents led to the change of both intensities and forms of most vibrations in IR and Raman spectra.

The structure of a CuPcCl $_4$ single crystal grown by sublimation in vacuum was refined for the first time. CuPcCl $_4$ was shown to crystallize in the monoclinic P2 $_1$ /c space group with the following unit cell parameters at 150 K: $Z = 2$, $a = 14.0052(9)$ Å, $b = 3.6376(3)$ Å, $c = 26.5123(18)$ Å, $\beta = 94.893(3)^\circ$.

The effect of chloro-substitution on the structure of CuPcCl $_x$ thin films deposited in vacuum onto the substrate at 50 and 200 °C was studied. It was shown that when deposited on a substrate at 50 °C, CuPcCl $_4$ formed polycrystalline films with the preferential orientation of the (100) crystallographic plane of crystallites parallel to the substrate surface and the inclination angle of molecules relative to the substrate surface of 79.2°. Introduction of more Cl-substituents into the phthalocyanine macrocycle led to the formation of amorphous films on the substrates at 50 °C. At elevated substrate temperatures, the growth of polycrystalline disordered films was observed for all three CuPcCl $_x$ ($x = 4, 8, 16$) phthalocyanines. These data can be used for the interpretation of correlations between the structure and properties of films when creating active layers of electronic devices based on chlorinated metal phthalocyanines.

Supplementary Materials: The following are available online, Table S1: Experimental and calculated IR wavenumbers (cm $^{-1}$) and assignments of the most intense vibrations in the IR spectrum of CuPcCl $_4$, Table S2: Experimental and calculated Raman shifts (cm $^{-1}$) and assignments of the most intense vibrations in the Raman spectrum of CuPcCl $_4$, Table S3: Experimental and calculated IR wavenumbers (cm $^{-1}$) and assignments of the most intense vibrations in the IR spectrum of CuPcCl $_8$, Table S4: Experimental and calculated Raman shifts (cm $^{-1}$) and assignments of the most intense vibrations in the Raman spectrum of CuPcCl $_8$, Table S5: Experimental and calculated Raman and IR wavenumbers (cm $^{-1}$) and assignments of the most intense vibrations in the IR and Raman spectrum of CuPcCl $_{16}$, Table S6: Measured peak positions, intensities and assigned hkl indexes for the XRD pattern of CuPcCl $_{16}$, Table S7: Measured peak positions, intensities and assigned hkl indexes for the XRD pattern of CuPcCl $_8$.

Author Contributions: Conceptualization, T.B. and P.K.; methodology, D.K.; software, P.K.; validation, A.S., T.B. and D.B.; formal analysis, P.K.; investigation, D.B., D.K. and A.S.; resources, T.B.; writing—original draft preparation, D.K. and A.S.; writing—review and editing, T.B.; visualization, D.B.; supervision, T.B.; project administration, T.B.; funding acquisition, T.B. All authors have read and agreed to the published version of the manuscript.

Funding: This research received no external funding.

Acknowledgments: The authors acknowledge the Ministry of Science and Higher Education (Russia) for administrative support.

Conflicts of Interest: The authors declare no conflict of interest.

References

1. Shigemitsu, M. Syntheses of Chlorinated Copper Phthalocyanines from Chlorophthalic Anhydrides. *Bull. Chem. Soc. Jpn.* **1959**, *32*, 691–693.
2. Abe, T.; Nagai, K. Novel photofunctions of bilayer composed of p-type phthalocyanine and n-type organic semiconductor as photoelectrodes in the water phase. *Org. Electron.* **2007**, *8*, 262–271.
3. Nénon, S.; Kanehira, D.; Yoshimoto, N.; Fages, F.; Vidélot-Ackermann, C. Shelf-life time test of p- and n-channel organic thin film transistors using copper phthalocyanines. *Thin Solid Films* **2010**, *518*, 5593–5598.
4. Bao, Z.; Lovinger, A.J.; Brown, J. New Air-Stable n-Channel Organic Thin Film Transistors. *J. Am. Chem. Soc.* **1998**, *120*, 207–208.
5. Ma, F.; Wang, S.; Li, X. Synthesis, spectral characterization of CuPcF16 and its application in organic thin film transistors using p-6p as inducing layer. *J. Phys. Chem. Solids* **2012**, *73*, 589–592.
6. Shao, X.; Wang, S.; Li, X.; Su, Z.; Chen, Y.; Xiao, Y. Single component p-, ambipolar and n-type OTFTs based on fluorinated copper phthalocyanines. *Dye. Pigment.* **2016**, *132*, 378–386.
7. Wu, F.-C.; Cheng, H.-L.; Yen, C.-H.; Lin, J.-W.; Liu, S.-J.; Chou, W.-Y.; Tang, F.-C. Electron transport properties in fluorinated copper-phthalocyanine films: Importance of vibrational reorganization energy and molecular microstructure. *Phys. Chem. Chem. Phys.* **2010**, *12*, 2098.
8. Oh, Y.; Pyo, S.; Yi, M.; Kwon, S.-K. N-type organic field-effect transistor using polymeric blend gate insulator with controlled surface properties. *Org. Electron.* **2006**, *7*, 77–84.
9. Klyamer, D.D.; Sukhikh, A.S.; Krasnov, P.; Gromilov, S.A.; Morozova, N.B.; Basova, T.V. Thin films of tetrafluorosubstituted cobalt phthalocyanine: Structure and sensor properties. *Appl. Surf. Sci.* **2016**, *372*, 79–86.
10. Parkhomenko, R.; Sukhikh, A.S.; Klyamer, D.D.; Krasnov, P.; Gromilov, S.; Kadem, B.; Hassan, A.K.; Basova, T.V. Thin Films of Unsubstituted and Fluorinated Palladium Phthalocyanines: Structure and Sensor Response toward Ammonia and Hydrogen. *J. Phys. Chem. C* **2017**, *121*, 1200–1209.
11. Klyamer, D.D.; Sukhikh, A.S.; Trubin, S.V.; Gromilov, S.A.; Morozova, N.B.; Basova, T.V.; Hassan, A.K. Tetrafluorosubstituted Metal Phthalocyanines: Interplay between Saturated Vapor Pressure and Crystal Structure. *Cryst. Growth Des.* **2020**, *20*, 1016–1024. [[CrossRef](#)]
12. Sharma, R.K.; Gulati, S.; Sachdeva, S. One pot and solvent-free synthesis of 2,9,16,23-tetrachlorometal(II) phthalocyanines. *Green Chem. Lett. Rev.* **2012**, *5*, 83–87. [[CrossRef](#)]
13. Safari, N.; Jamaat, P.R.; Pirouzmand, M.; Shaabani, A. Synthesis of metallophthalocyanines using microwave irradiation under solvent free and reflux conditions. *J. Porphyrins Phthalocyanines* **2004**, *8*, 1209–1213. [[CrossRef](#)]
14. Safari, N.; Jamaat, P.R.; Shirvan, S.A.; Shoghpour, S.; Ebadi, A.; Darvishi, M.; Shaabani, A. Rapid and efficient synthesis of metallophthalocyanines in ionic liquid. *J. Porphyrins Phthalocyanines* **2005**, *9*, 256–261. [[CrossRef](#)]
15. Lomova, T.N.; Sokolova, T.N.; Zaitseva, S.; Zdanovich, S.; Maizlish, V.E. Structure and properties of tetrakis(3(4)-chlorophthalocyaninato)copper(II) protonated forms in the isolated state and in the sulfuric acid solutions. *Russ. J. Gen. Chem.* **2013**, *83*, 1563–1570. [[CrossRef](#)]
16. Zięba-Palus, J.; Michalska, A. Characterization of Blue Pigments Used in Automotive Paints by Raman Spectroscopy. *J. Forensic Sci.* **2014**, *59*, 943–949. [[CrossRef](#)]
17. Duce, C.; Della Porta, V.; Tiné, M.R.; Spepi, A.; Ghezzi, L.; Colombini, M.P.; Bramanti, E. FTIR study of ageing of fast drying oil colour (FDOC) alkyd paint replicas. *Spectrochim. Acta Part. A: Mol. Biomol. Spectrosc.* **2014**, *130*, 214–221. [[CrossRef](#)]

18. Pakhomov, L.G.; Pakhomov, G.L. NO₂ interaction with thin film of phthalocyanine derivatives {1}. *Synth. Met.* **1995**, *71*, 2299–2300. [[CrossRef](#)]
19. Irie, S.; Hoshino, A.; Kuwamoto, K.; Isoda, S.; Miles, M.; Kobayashi, T. Point-on-line coincidence in epitaxial growth of CuPcCl₁₆ on graphite. *Appl. Surf. Sci.* **1997**, *113*, 310–315. [[CrossRef](#)]
20. Mittelberger, A.; Kramberger, C.; Meyer, J.C. Insights into radiation damage from atomic resolution scanning transmission electron microscopy imaging of mono-layer CuPcCl₁₆ films on graphene. *Sci. Rep.* **2018**, *8*, 4813. [[CrossRef](#)]
21. Yoshida, K.; Biskupek, J.; Kurata, H.; Kaiser, U. Critical conditions for atomic resolution imaging of molecular crystals by aberration-corrected HRTEM. *Ultramicroscopy* **2015**, *159*, 73–80. [[CrossRef](#)]
22. Bobaru, S.C.; Salomon, E.; Layet, J.-M.; Angot, T. Structural Properties of Iron Phthalocyanines on Ag(111): From the Submonolayer to Monolayer Range. *J. Phys. Chem. C* **2011**, *115*, 5875–5879. [[CrossRef](#)]
23. Amsalem, P.; Giovanelli, L.; Themlin, J.M.; Koudia, M.; Abel, M.; Oison, V.; Ksari, Y.; Mossoyan, M.; Porte, L. Interface formation and growth of a thin film of ZnPcCl₈/Ag(111) studied by photoelectron spectroscopy. *Surf. Sci.* **2007**, *601*, 4185–4188. [[CrossRef](#)]
24. Haruta, M.; Kurata, H. Direct observation of crystal defects in an organic molecular crystals of copper hexachlorophthalocyanine by STEM-EELS. *Sci. Rep.* **2012**, *2*, 252. [[CrossRef](#)] [[PubMed](#)]
25. Fryer, J.R. Electron Crystallography of Phthalocyanines. *J. Porphyr. Phthalocyanine* **1999**, *3*, 672–678. [[CrossRef](#)]
26. Selvaraj, T.; Rajalingam, R. Theoretical Studies of the Zeolite-Y Encapsulated Chlorine-Substituted Copper(II)phthalocyanine Complex on the Formation Glycidol from Allyl Alcohol. *ACS Omega* **2018**, *3*, 9613–9619. [[CrossRef](#)] [[PubMed](#)]
27. Sahoo, S.R.; Sahu, S.; Sharma, S. Charge transport and prototypical optical absorptions in functionalized zinc phthalocyanine compounds: A density functional study. *J. Phys. Org. Chem.* **2017**, *31*, e3785. [[CrossRef](#)]
28. Koshy, R.; Menon, C.S. Influence of air annealing and gamma ray irradiation on the optical properties of Cl₁₆FePc thin films. *E-Journal Chem.* **2012**, *9*, 2439–2445. [[CrossRef](#)]
29. Achar, B.N.; Jayasree, P.K. “Molecular Metals” Based on Copper(II) 2,9,16,23-tetrahalo Substituted Phthalocyanine Derivatives. *Synth. React. Inorg. Met. Chem.* **2000**, *30*, 719–733. [[CrossRef](#)]
30. Ling, M.-M.; Bao, Z.; Erk, P. Air-stable n-channel copper hexachlorophthalocyanine for field-effect transistors. *Appl. Phys. Lett.* **2006**, *89*, 163516. [[CrossRef](#)]
31. Honigmann, B.; Lenne, H.U.; Schrödel, R.; Anilin, B. Beziehungen zwischen den strukturen der modifikationen des platin- und kupferphthalocyanins und einiger chlorderivate. *Zeitschrift für Krist. - New Cryst. Struct.* **1965**, *122*, 185–205.
32. Brown, C.J. Crystal structure of β-copper phthalocyanine. *J. Chem. Soc. A* **1968**, 2488. [[CrossRef](#)]
33. Erk, P.; Hengelsberg, H.; Haddow, M.; Van Gelder, R. The innovative momentum of crystal engineering. *CrystEngComm* **2004**, *6*, 474. [[CrossRef](#)]
34. Basova, T.V.; Kiselev, V.; Schuster, B.-E.; Peisert, H.; Chassé, T. Experimental and theoretical investigation of vibrational spectra of copper phthalocyanine: Polarized single-crystal Raman spectra, isotope effect and DFT calculations. *J. Raman Spectrosc.* **2009**, *40*, 2080–2087. [[CrossRef](#)]
35. Uyeda, N. Molecular image resolution in electron microscopy. *J. Appl. Phys.* **1972**, *43*, 5181. [[CrossRef](#)]
36. Ruffer, T.; Nurpeisova, D.; Jakupova, Z.; Tashenov, A.; Uhlig, N.; Khalladi, A.; Mertens, L.; Gonser, A.; Mehring, M.; Lang, H. Synthesis and purification of metalloctachlorophthalocyanines. *Zeitschrift für Naturforschung B* **2017**, *72*, 589–601. [[CrossRef](#)]
37. Louër, D.; Boulitif, A. Some further considerations in powder diffraction pattern indexing with the dichotomy method. *Powder Diffr.* **2014**, *29*, S7–S12. [[CrossRef](#)]
38. Jiang, H.; Hu, P.; Ye, J.; Li, Y.; Li, H.; Zhang, X.; Li, R.; Dong, H.; Hu, W.; Kloc, C. Molecular Crystal Engineering: Tuning Organic Semiconductor from p-type to n-type by Adjusting Their Substitutional Symmetry. *Adv. Mater.* **2017**, *29*, 1605053. [[CrossRef](#)]
39. Klyamer, D.D.; Sukhikh, A.S.; Gromilov, S.A.; Kruchinin, V.N.; Spesivtsev, E.V.; Hassan, A.K.; Basova, T.V. Influence of Fluorosubstitution on the Structure of Zinc Phthalocyanine Thin Films. *Macroheterocycles* **2018**, *11*, 304–311. [[CrossRef](#)]
40. APEX3; v.2018-7.2; Bruker AXS, Inc.: Madison, WI, USA, 2018.
41. Dolomanov, O.; Bourhis, L.J.; Gildea, R.; Howard, J.A.; Puschmann, H. OLEX2: A complete structure solution, refinement and analysis program. *J. Appl. Crystallogr.* **2009**, *42*, 339–341. [[CrossRef](#)]

42. Sheldrick, G.M. SHELXT - integrated space-group and crystal-structure determination. *Acta Crystallogr. Sect. A Found. Adv.* **2015**, *71*, 3–8. [[CrossRef](#)]
43. Sheldrick, G.M. Crystal structure refinement with SHELXL. *Acta Crystallogr. Sect. C Struct. Chem.* **2015**, *71*, 3–8. [[CrossRef](#)]
44. Jayatilaka, D.; Wolff, S.K.; Grimwood, D.J.; McKinnon, J.J.; Spackman, M.A. CrystalExplorer: A tool for displaying Hirshfeld surfaces and visualising intermolecular interactions in molecular crystals. *Acta Crystallogr. Sect. A Found. Crystallogr.* **2006**, *62*, s90. [[CrossRef](#)]
45. Jayatilaka, D.; Grimwood, D. Tonto: A Fortran Based Object-Oriented System for Quantum Chemistry and Crystallography. *Computer Vision* **2003**, *2660*, 142–151.
46. Becke, A.D. Density-functional thermochemistry. III. The role of exact exchange. *J. Chem. Phys.* **1993**, *98*, 5648–5652. [[CrossRef](#)]
47. Hehre, W.J. Self-Consistent Molecular Orbital Methods. XII. Further Extensions of Gaussian-Type Basis Sets for Use in Molecular Orbital Studies of Organic Molecules. *J. Chem. Phys.* **1972**, *56*, 2257. [[CrossRef](#)]
48. Hariharan, P.C.; Pople, J.A. The influence of polarization functions on molecular orbital hydrogenation energies. *Theor. Chem. Accounts* **1973**, *28*, 213–222. [[CrossRef](#)]
49. Rassolov, V.; Windus, T.L.; Pople, J.A.; Ratner, M.A. 6-31G* basis set for atoms K through Zn. *J. Chem. Phys.* **1998**, *109*, 1223–1229. [[CrossRef](#)]
50. Schmidt, M.W.; Baldridge, K.K.; Boatz, J.A.; Elbert, S.; Gordon, M.S.; Jensen, J.H.; Koseki, S.; Matsunaga, N.; Nguyen, K.A.; Su, S.; et al. General atomic and molecular electronic structure system. *J. Comput. Chem.* **1993**, *14*, 1347–1363. [[CrossRef](#)]

Sample Availability: Samples of the compounds of CuPcCl₄, CuPcCl₈ and CuPcCl₁₆ are available from the authors.



© 2020 by the authors. Licensee MDPI, Basel, Switzerland. This article is an open access article distributed under the terms and conditions of the Creative Commons Attribution (CC BY) license (<http://creativecommons.org/licenses/by/4.0/>).